Search for Squarks and Gluinos in the Jets + Missing E_T Topology with the DØ Detector

The DØ Collaboration
URL: http://www-d0.fnal.gov
Contact Person for This Analysis: pverdier@fnal.gov

Draft Version 1.6

(Dated: March 3, 2005)

A search for squarks and gluinos has been performed on $310\,\mathrm{pb}^{-1}$ of data from p$\bar{\mathrm{p}}$ collisions at a center-of-mass energy of 1.96 TeV, collected by the DØ detector at the Fermilab Tevatron. The topology analyzed consists of jets with large missing E_T. The data show good agreement with the standard model expectations. Improved mass limits for squarks and gluinos have been derived in the framework of minimal supergravity.

Preliminary Results for Winter 2005 Conferences

I. INTRODUCTION

Topologies involving jets and missing transverse energy have been widely investigated in the past to search for signals of new phenomena in p$\bar{\text{p}}$ collisions. In this note, a search for squarks and gluinos in the jets with large missing E_T ($\not{E}_T$) topology is reported, using $310\,\text{pb}^{-1}$ of data collected at a center-of-mass energy of $1.96\,\text{TeV}$ with the upgraded DØ detector during Run II of the Fermilab Tevatron.

In models based on theories of supersymmetry, scalar quarks, or squarks, arise as partners of the ordinary quarks and fermionic gluinos as partners of the ordinary gluons. Supersymmetric particles carry a value of -1 for R-parity, a multiplicative quantum number. In R-parity conserving theories, supersymmetric particles are therefore produced in pairs. Their decay leads to standard model (SM) particles and, possibly *via* cascades, to the lightest supersymmetric particle (LSP) which is stable. The widely preferred LSP candidate is the lightest neutralino χ, which is weakly interacting and escapes detection. (The neutralinos are the supersymmetric partners of the neutral gauge and Higgs bosons.)

At hadron colliders, the most copiously produced supersymmetric particles should be, if sufficiently light, colored particles, namely squarks and gluinos. If squarks are lighter than gluinos, they will tend to decay according to $\tilde{\text{q}} \to \text{q}\chi$, and their pair production will yield an acoplanar jet topology with missing E_T carried away by the two neutralino LSP's. If gluinos are lighter than squarks on the other hand, their pair production and decay *via* $\tilde{\text{g}} \to \text{q}\bar{\text{q}}\chi$ will lead to topologies containing a large number of jets and missing E_T. In generic models, squarks of the five lightest flavors tend to be of similar masses. The same is true for the supersymmetric partners of both quark helicity states. Hence, the cross section of squark pair production corresponds effectively to the sum of the productions of ten squark species.

In this note, squark and gluino production is investigated in the framework of minimal supergravity (mSUGRA) [3]. The current mass limits are of the order of $195\,\text{GeV}/c^2$ for gluinos with heavy squarks, and $300\,\text{GeV}/c^2$ for squarks and gluinos of equal masses [1, 2]. Here and in the following, all limits are at the 95% confidence level (CL). All results reported are preliminary.

II. DATA SAMPLE

For the studies reported in this note, an integrated luminosity of $\sim 350\,\text{pb}^{-1}$, collected from April 2003 through August 2004, has been analyzed. The Jets $+ \not{E}_T$ trigger used was not available previously in Run II. At the first level (L1), the trigger selects events in which at least three calorimeter trigger towers record a transverse energy in excess of $5\,\text{GeV}$. At the second (L2) and third trigger levels (L3), requirements are placed on $\not{H}_T$, the missing transverse energy to the reconstructed jets ($\not{H}_T = |\sum_{jets} \vec{p}_T|$). The $\not{H}_T$ thresholds are 20 and $30\,\text{GeV}$ at Levels 2 and 3, respectively. For data collected after June 2004, the acoplanarity $\Delta\Phi$ (azimuthal angle between the two leading jets) is required to be lower than 168.75 degrees at L2 and lower than 170 degrees at L3. An extra cut at L3 also requires H_T to be greater than $50\,\text{GeV}$ ($H_T = \sum_{jets} |\vec{p}_T|$).

For the subsequent data selection, it was required that no major component of the detector show any sign of degraded performance. This leaves an available total integrated luminosity of $310\,\text{pb}^{-1}$. The offline analysis utilizes jets reconstructed with the Run II cone algorithm, with a radius of 0.5 in η-ϕ space, appropriately corrected for the jet energy scale. The so-called good jets are further selected by general quality criteria essentially based on the jet transverse and longitudinal profiles.

The sample of ~ 37 million events collected with the Jets $+ \not{E}_T$ trigger was reduced to a more manageable size by requiring the following criteria to be satisfied:

- $\not{H}_T > 40\,\text{GeV}$;

- at least two jets;

- $\not{E}_T > 40\,\text{GeV}$;

- $\Delta\Phi < 165°$.

Here and in the following, the qualifier "good" in front of "jet" is dropped; it will be restored only in the cases of ambiguities. Only good jets enter the calculation of kinematic quantities such as $\not{H}_T$ or H_T.

Events in which the presence of obvious calorimeter noise could be detected were rejected, as well as those containing at least one jet not rated as good and with a transverse energy larger than $15\,\text{GeV}$. The inefficiency of 3.9% associated with these criteria was measured on events selected at random beam crossings (zero-bias events), and also on events collected with an unbiased trigger and containing exactly two jets back-to-back in Φ within $15°$.
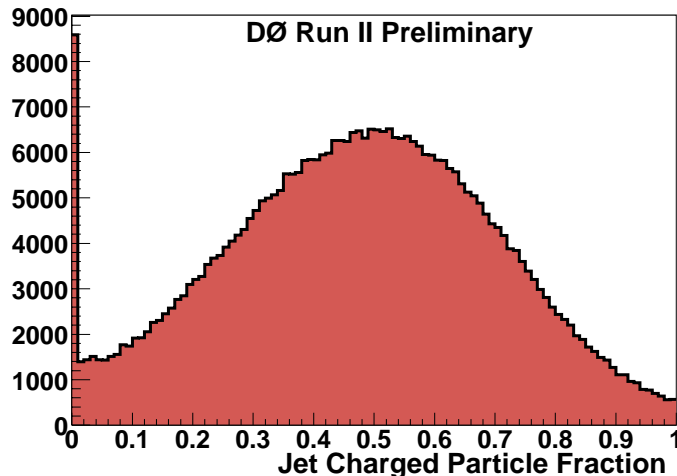
FIG. 1: Distribution of the charged particle fraction CPF for central jets.

This sample is still dominated by QCD events with jet transverse energy mismeasurements. Such mismeasurements can in particular be due to a wrong vertex choice, or to cosmic rays showering in the calorimeter. The improved tracking capabilities of the upgraded DØ detector can be used to largely reduce these backgrounds.

First the longitudinal position z of the vertex is restricted to ensure an efficient primary vertex reconstruction: $|z| < 60$ cm. This cut removes 3.9% of the events.

Then, the two leading jets are required to be in the central region of the calorimeter, with $|\eta_{\mathrm{det}}| < 0.8$. (Here, η_{det} is the jet pseudorapidity, assuming that the jet originates from the detector center.) They must be hadronic, with an electromagnetic fraction $EMF < 0.95$. Cuts on P_t at 60 GeV/c and 40 GeV/c are applied on the first and second leading jet, respectively.

Next a comparison of jet energies with their counterparts carried by charged particles is performed. The ratio CPF of the transverse energy carried by the charged particles associated with a jet to its transverse energy recorded in the calorimeter is expected to be close to zero if a wrong primary vertex was selected. In such a case, it is unlikely that the charged tracks truly associated to the jet will emanate from the selected primary vertex. Furthermore, if the jet is a fake one, there should be no real charged tracks associated with it, and its CPF should also be close to zero. The CPF distribution is shown in Fig. 1 for jets in events selected with an unbiased trigger. A jet is hereafter considered "confirmed" if its CPF is larger than 0.05.

The inefficiency of this jet confirmation procedure was determined using back-to-back dijet events with both jets required to be central ($|\eta_{\mathrm{det}}| < 1$). From the fractions of events with 0, 1, or 2 jets confirmed, it is deduced that the chosen vertex is the correct one in 99% of the cases, and that track confirmation of a jet then occurs at a rate of 98% within $|\eta_{\mathrm{det}}| < 1$. It has been checked that this efficiency does not depend on the jet p_T within the range of interest for the analysis reported in this note.

III. SIMULATED SAMPLES

Signal efficiencies and non-QCD standard model backgrounds have been evaluated using fully simulated and reconstructed Monte Carlo events, in which the jet energies received an additional smearing to take into account the different resolutions in data and Monte Carlo. The QCD background has not been simulated, and was estimated directly from the data.

A. Standard model background simulation

The processes listed in Table I are expected to be the largest contributors to standard model backgrounds in the jets + missing E_T topology. They were generated with ALPGEN [4], interfaced with PYTHIA [5] for the simulation of initial and final state radiation and of jet hadronization. The parton density functions (PDF's) used were CTEQ5L [6], depending on the process. An average of 0.8 minimum bias events was superimposed. The next-to-leading order

TABLE I: Standard model processes, numbers of events generated and cross sections. $t\bar{t}$ cross section has been taken from [8].

SM process	mass cut GeV/c^2	events generated	cross section pb
$Z \to \nu\bar{\nu} + 2j$	-	20,000	174.
$Z \to \nu\bar{\nu} + 3j$	-	36,000	54.2
$Z \to \nu\bar{\nu} + 4j$	-	10,000	16.1
$W \to \tau\nu + 2j$	-	28,500	287.7
$W \to \mu\nu + 2j$	-	51,750	287.7
$W \to e\nu + 2j$	-	53,500	287.7
$Z/\gamma^* \to \tau\tau + 2j$	[10-15]	5,750	31.0
$Z/\gamma^* \to \tau\tau + 2j$	[15-60]	2,000	26.2
$Z/\gamma^* \to \tau\tau + 2j$	[60-130]	38,750	28.3
$Z/\gamma^* \to \mu\mu + 2j$	[10-15]	17,750	31.0
$Z/\gamma^* \to \mu\mu + 2j$	[15-60]	18,000	26.2
$Z/\gamma^* \to \mu\mu + 2j$	[60-130]	58,750	28.3
$Z/\gamma^* \to ee + 2j$	[10-15]	32,250	31.0
$Z/\gamma^* \to ee + 2j$	[15-60]	36,750	26.2
$Z/\gamma^* \to ee + 2j$	[60-130]	110,000	28.3
$t\bar{t} \to b\bar{b}jjjj$	-	9,500	3.09
$t\bar{t} \to b\bar{b}jjl\nu$	-	142,300	2.92
$t\bar{t} \to b\bar{b}l\nu l\nu$	-	57,500	0.69

(NLO) cross sections were computed with MCFM [7].

B. Signal simulation

The production of squarks and gluinos *via* the processes

$$q\bar{q} \text{ or } gg \to \tilde{q}\bar{\tilde{q}} \text{ or } \tilde{g}\tilde{g}$$

$$qq \to \tilde{q}\tilde{q}$$

$$qg \to \tilde{q}\tilde{g}$$

was simulated using PYTHIA with the CTEQ5L PDF's. An average of 0.8 minimum bias events was overlaid.

The mSUGRA parameters were chosen at the boundary of the DØ [1] and CDF [2] Run I exclusion domain for $\tan\beta = 3$, $A_0 = 0$, $\mu < 0$. Three configurations are studied and there will be a dedicated analysis for each of them (Table II):

- "dijet" analysis :
  At low m_0, the gluino is heavier than the squarks. The process with the dominant cross section is the $\tilde{q}\bar{\tilde{q}}$ production. The analysis is optimized to search for acoplanar dijet events. m_0 was fixed at 25 GeV/c^2 and $m_{1/2}$ was incremented from 100 to 160 GeV/c^2 with a 5 GeV/c^2 step.

- "gluino" analysis:
  At high m_0, the squarks are much heavier than the gluino. The process with the highest cross section is therefore $\tilde{g}\tilde{g}$. The analysis is optimized to search for multijets events (≥ 4 jets). m_0 was fixed at 500 GeV/c^2 and $m_{1/2}$ was incremented from 65 GeV/c^2 to 90 GeV/c^2 with a 5 GeV/c^2 step.

- "3 jets" analysis:
  In the intermediate m_0 region, all squark-gluino production processes contribute to the total cross section, especially the $\tilde{q}\tilde{g}$ process becomes important. The analysis is optimized to search for events with at least 3 jets. The benchmark for this analysis is the particular case where $M_{\tilde{q}} = M_{\tilde{g}}$. Samples fulfilling this condition were generated between 290 and 340 GeV/c^2 with a 5 GeV/c^2 step.

For the production, only squarks belonging to the first two generations and the two sbottom squarks were considered. The average squark mass $M_{\tilde{q}}$ used in this note is therefore the average mass of all squarks without the two stop squarks. The version 7.58 of ISAJET [10] was used to calculate physical masses, PYTHIA 6.202 to compute leading order (LO) cross sections and to generate events, and PROSPINO [9] to obtain NLO K-factors for the

TABLE II: Chosen $m_{1/2}$ values, corresponding average-squark and gluino masses in GeV/c^2, and total squark-and-gluino production cross sections (pb).

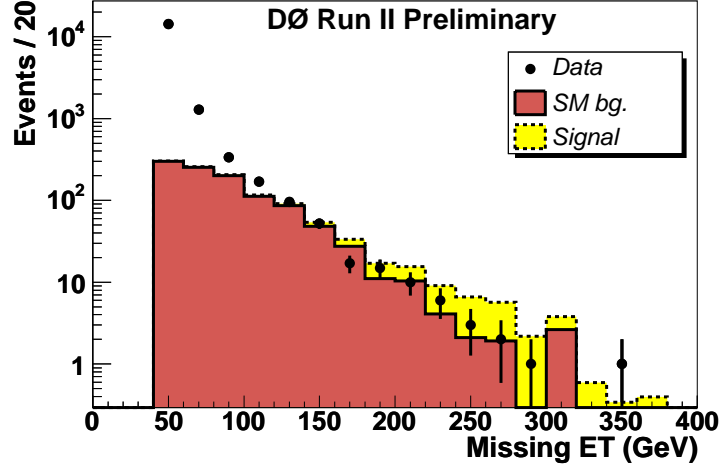| "dijet" analysis				"gluino" analysis				"3 jets" analysis			
$(m_0, m_{1/2})$	$m_{\tilde{q}}$	$m_{\tilde{g}}$	σNLO	$(m_0, m_{1/2})$	$m_{\tilde{q}}$	$m_{\tilde{g}}$	σNLO	$(m_0, m_{1/2})$	$m_{\tilde{q}}$	$m_{\tilde{g}}$	σNLO
(25,100)	227	260	9.80	(500,65)	497	203	7.72	(170,109)	290	290	2.00
(25,105)	237	270	7.32	(500,70)	500	215	5.18	(172,111)	295	295	1.75
(25,110)	248	284	5.19	(500,75)	504	228	3.24	(175,113)	300	300	1.48
(25,115)	258	296	3.88	(500,80)	507	240	2.25	(179,115)	305	305	1.27
(25,120)	268	306	2.91	(500,85)	511	251	1.57	(178,118)	310	310	1.14
(25,125)	278	319	2.17	(500,90)	514	265	1.03	(180,120)	315	315	0.99
(25,130)	288	332	1.58					(184,122)	320	320	0.85
(25,135)	297	340	1.25					(188,124)	325	325	0.74
(25,140)	308	353	0.92					(191,126)	330	330	0.64
(25,145)	318	366	0.68					(195,128)	335	335	0.55
(25,150)	328	378	0.52					(199,130)	340	340	0.48
(25,155)	337	386	0.41								
(25,160)	347	399	0.30								

FIG. 2: Distributions after the pre-selection for data (points with error bars), for non-QCD Standard Model background (full histogram), and for signal Monte Carlo (point from the "dijet" analysis with $(m_0, m_{1/2})$=(25,145) GeV/c^2; dashed histogram on top of SM).

various production processes. All decay channels are implemented in the generator, including cascade decays such as $\tilde{q} \to \chi^+ q \to qqq\chi$.

IV. EVENT SELECTION

A. pre-selection

The $\not{E}_T$ distribution after the common pre-selection described in section II is shown Fig. 2. It can be observed that the QCD-background increases rapidly for $\not{E}_T$ below 100 GeV. On the other side, the tail of the $\not{E}_T$ distribution is well described by the SM background contributions alone.

B. "dijet" analysis

The selection cuts for the "dijet" analysis are summarized in Table III. After the common pre-selection step, the cut on the P_t of the second leading jet is reinforced at $50\,\mathrm{GeV}/c$. $\not{E}_T$ is required to be greater than $60\,\mathrm{GeV}$ to remove QCD background far away from the final $\not{E}_T$ cut. Then, a veto on isolated electrons and muons (cut **DI3** and **DI4**) rejects a large fraction of events originating from the W/Z + jet(s) processes. The cuts **DI5** and **DI6** are intended to remove events where the energy of one jet fluctuated, generating $\not{E}_T$ aligned to that jet. The minimal azimuthal angle between any jets and the $\not{E}_T$ is required to be greater than 30 degrees. In addition, the azimuthal angle between the second leading jet and the $\not{E}_T$ to be greater than 50 degrees. The final cuts **DI7** and **DI8** are then performed. For various combinations of cut values on $\not{E}_T$ and H_T, the expected cross section upper limit $\mathcal{S}$ for $m_{1/2} = 130\,\mathrm{GeV}/c^2$ was determined, assuming that the number of events observed would be the one expected from background, and taking the systematic uncertainties discussed further down into account. The optimal set of cuts is the one which minimizes $\mathcal{S}$:

- $\not{E}_T > 175\,\mathrm{GeV}$;

- $H_T > 250\,\mathrm{GeV}$.

The number of events remaining at each step is given in Table III. The marginal distribution of H_T and $\not{E}_T$ (all cuts applied except the cut on the considered variable, **DI7** and **DI8** respectively) are shown on Fig. 3. Twelve events were selected in the data.

The various Standard Model background contributions are listed in Table IV. The main contributor is, as expected, $Z \to \nu\bar{\nu} + \mathrm{jet\,jet}$. The QCD background above the $\not{E}_T$ cut at $175\,\mathrm{GeV}$ is found to be totally negligible. It is therefore conservatively neglected.

The signal efficiencies were evaluated using fully simulated events. The evolution of the efficiency at the various stages of the analysis is given in Table III for $(m_0, m_{1/2}) = (25, 145)\,\mathrm{GeV}/c^2$, together with the numbers of events seen in the data. The final efficiencies for various $m_{1/2}$ values are displayed in Table V. To avoid statistical fluctuations, these efficiencies are fitted with a straight line as a function of the squark mass (Fig. 4). In the limit computation, the efficiency from the fit will be used rather than the single point efficiency.
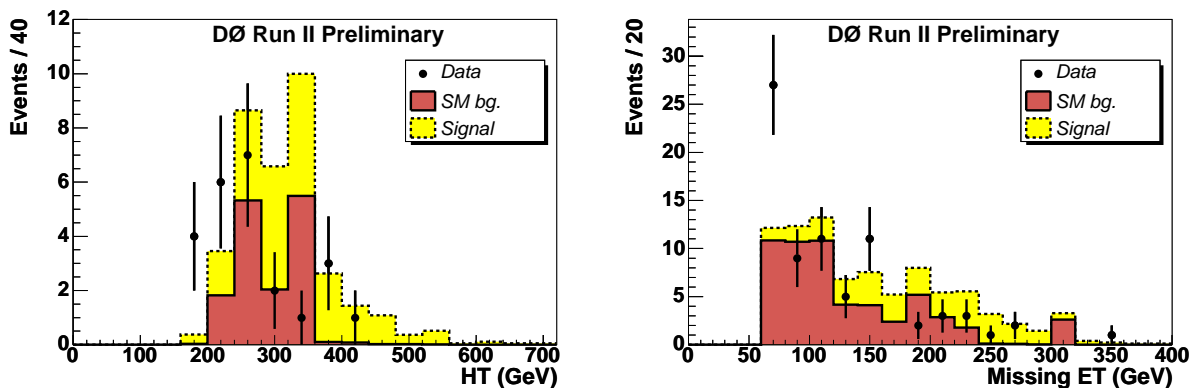

FIG. 3: "dijet" analysis : Marginal distribution of H_T (left) and $\not{E}_T$ (right) for data (points with error bars), for non-QCD standard model background (full histogram), and for signal Monte Carlo ($m_{1/2} = 145\,\mathrm{GeV}/c^2$; dashed histogram on top of SM).

TABLE III: Number of data events and signal efficiencies for $(m_0, m_{1/2}) = (25, 145)$ GeV/c^2 at the various stages of the "dijet" analysis.

cut applied	events left	efficiency (%)
Common pre-selection	18,149	30.3
DI1: 2nd leading jet $P_t > 50$ GeV/c	12,778	29.2
DI2: $\not{E}_T > 60$ GeV	1,539	28.1
DI3: EM veto	1,394	23.6
DI4: Muon veto	1,293	18.1
DI5: $\Delta\Phi min(MET, any\,jet) > 30$ degrees	408	14.7
DI6: $\Delta\Phi(MET, jet2) > 50$ degrees	313	14.1
DI7: $H_T > 250$ GeV	75	11.7
DI8: $\not{E}_T > 175$ GeV	12	7.1

TABLE IV: Standard model processes and numbers of events expected in the "dijet" analysis. The errors on the numbers of events expected are statistical only.

SM process	events expected
Z $\to \nu\bar{\nu}$ + jet jet	5.2 ± 3.7
W $\to \tau\nu$ + jet jet	3.0 ± 3.0
W $\to \mu\nu$ + jet jet	1.7 ± 1.7
W $\to$ eν + jet jet	1.6 ± 1.6
t$\bar{\text{t}} \to$ b$\bar{\text{b}}$jjlν	1.4 ± 0.1
t$\bar{\text{t}} \to$ b$\bar{\text{b}}$lνlν	0.02 ± 0.01
QCD	negligible
total	12.8 ± 5.4

TABLE V: Signal efficiencies and number of events expected in the "dijet" analysis. The errors are statistical only.

$(m_0, m_{1/2})$ (GeV/c^2)	efficiency (%)	events expected
(25,100)	1.83 ± 0.19	55.6 ± 5.8
(25,105)	2.48 ± 0.22	56.2 ± 5.0
(25,110)	3.32 ± 0.25	53.5 ± 4.1
(25,115)	3.45 ± 0.26	41.5 ± 3.1
(25,120)	3.86 ± 0.27	34.8 ± 2.5
(25,125)	5.00 ± 0.31	33.6 ± 2.1
(25,130)	5.47 ± 0.32	26.8 ± 1.6
(25,135)	5.46 ± 0.32	21.2 ± 1.2
(25,140)	6.28 ± 0.35	17.9 ± 1.0
(25,145)	6.83 ± 0.38	14.4 ± 0.8
(25,150)	6.95 ± 0.37	11.2 ± 0.6
(25,155)	8.10 ± 0.40	10.3 ± 0.5
(25,160)	8.17 ± 0.43	7.6 ± 0.4

C. "gluino" analysis

The selection cuts for the "gluino" analysis are summarized in Table VI. After the common pre-selection step, events are required to contain at least four jets. As for the two first jets, the third and fourth jets must be in the central region of the calorimeter ($|\eta_{\text{det}}| < 0.8$), confirmed by tracks ($CPF \geq 0.05$) and be hadronic ($EMF < 0.95$). P_t cuts at 30 GeV/c and 20 GeV/c are applied on the third and fourth leading jet respectively. The veto on isolated electrons and muons is performed. The cuts **GL12** and **GL13** are intended to remove events where the energy of one jet fluctuated, generating $\not{E}_T$ aligned to that jet. The cut on the minimum azimuthal angle between any jets and the $\not{E}_T$ performed in the "dijet" analysis (cut **DI5**) has been replaced by cut **GL12** on the azimuthal angle between
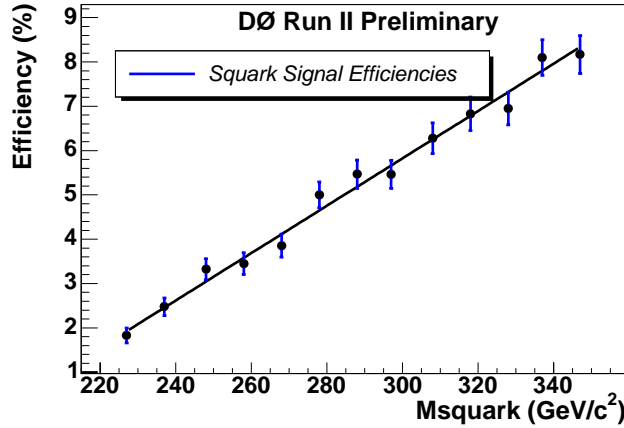
FIG. 4: Signal efficiencies in the "dijet" analysis as a function of the squark mass. The efficiency is fitted with a straight line.

the first leading jet and the $\not{E}_T$ at 90 degrees. This cut removes less background than **DI5**, but allow to keep large signal efficiencies. Finally, H_T is required to be greater than 250 GeV and $\not{E}_T$ greater than 75 GeV. The number of events remaining at each step is given in Table VI. Ten events were selected in the data.

The various Standard Model background contributions are listed in table VII. The main contributor is $t\bar{t} \rightarrow b\bar{b}jjl\nu$. The marginal distributions of H_T and $\not{E}_T$ are shown on Fig. 5. On the $\not{E}_T$ distribution, it can be seen that the QCD background increases rapidly outside of the region selected by the analysis cut (75 GeV). The separation between QCD and SM backgrounds is particularly clear. An exponential fit to the regions $40 < \not{E}_T < 60$ GeV is used to estimate the QCD contribution beyond the analysis cuts (75 GeV). The error on this QCD contribution is determined by varying by 1σ the parameters of the exponential function. A systematic error is determined by restricting the fit to the $[40, 55]$ GeV range in $\not{E}_T$. The result is $N_{QCD} = 1.6 \pm 0.2(stat.) \pm 0.4(syst.)$.

The evolution of the signal efficiency at the various stages of the analysis is given in Table VI for $m_{1/2} = 80$ GeV/c^2, together with the numbers of events seen in the data. The final efficiencies for various $m_{1/2}$ values are displayed in Table VIII. As the signal efficiencies are low, which can induce large statistical fluctuations, they are fitted with a 2nd order polynomial as a function of the gluino mass (Fig. 6). In the limit computation, the efficiency from the fit will be used rather than the single point efficiency.
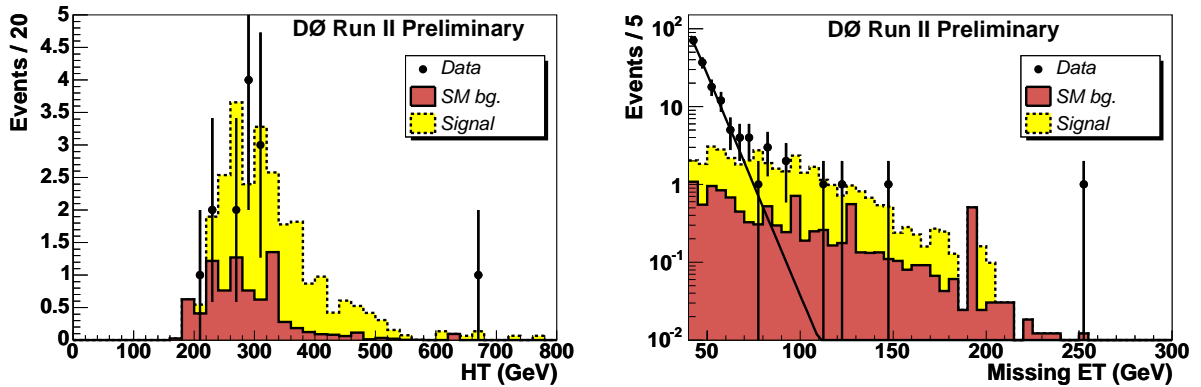

FIG. 5: "gluino" analysis : Marginal distributions of H_T (left) and $\not{E}_T$ (right) for non-QCD standard model background (full histogram), and for signal Monte Carlo $((m_0, m_{1/2}) = (500, 80)$ GeV/c^2; dashed histogram on top of SM). For the $\not{E}_T$ distribution, the fitted QCD background is also drawn.

TABLE VI: Number of data events and signal efficiencies for $(m_0, m_{1/2}) = (500, 80)$ GeV/c^2 at the various stages of the "gluino" analysis.

cut applied	events left	efficiency (%)
Common pre-selection	18,149	26.3
GL1 : at least 4 jets	9,216	24.6
GL2 : 3rd leading jet $|\eta_{\mathrm{det}}| < 0.8$	4,143	15.6
GL3 : 4th leading jet $|\eta_{\mathrm{det}}| < 0.8$	1,576	8.9
GL4 : 3rd leading jet CPF > 0.05	1,558	8.9
GL5 : 4th leading jet CPF > 0.05	1,527	8.9
GL6 : 3rd leading jet $P_t > 30$ GeV/c	1,115	8.3
GL7 : 4th leading jet $P_t > 20$ GeV/c	773	7.7
GL8 : 3rd leading jet EMF < 0.95	761	7.5
GL9 : 4th leading jet EMF < 0.95	746	7.2
GL10: EM veto	732	6.8
GL11: Muon veto	717	6.3
GL12: $\Delta\Phi(MET, jet1) > 90$ degrees	656	5.6
GL13: $\Delta\Phi(MET, jet2) > 50$ degrees	282	4.5
GL14: $H_T > 250$ GeV	188	4.1
GL15: $\not{E}_T > 75$ GeV	10	2.5

TABLE VII: Standard model processes and numbers of events expected in the "gluino" analysis. The errors on the numbers of events expected are statistical only.

SM process	events expected
$Z \to \nu\bar{\nu} + 4$jets	1.4 ± 0.8
$t\bar{t} \to b\bar{b}jjlnu$	3.7 ± 0.1
$t\bar{t} \to b\bar{b}lnulnu$	0.03 ± 0.01
$t\bar{t} \to b\bar{b}jjjj$	0.4 ± 0.2
QCD	1.6 ± 0.2
total	7.1 ± 0.9

TABLE VIII: Signal efficiencies and number of events expected in the "gluino" analysis. The errors are statistical only.

$(m_0, m_{1/2})$ (GeV/c^2)	efficiency (%)	events expected
(500,65)	1.10 ± 0.10	26.4 ± 2.5
(500,70)	1.12 ± 0.11	18.0 ± 1.7
(500,75)	1.61 ± 0.13	16.2 ± 1.3
(500,80)	2.38 ± 0.16	16.6 ± 1.1
(500,85)	2.22 ± 0.14	10.8 ± 0.7
(500,90)	2.91 ± 0.16	9.3 ± 0.5

D. "3 jets" analysis

The selection cuts for the "3 jets" analysis are summarized in Table IX. After the common pre-selection step, events are required to contain at least three jets. Like the first two jets, the third jet must be in the central region of the calorimeter ($|\eta_{\mathrm{det}}| < 0.8$), confirmed by tracks ($CPF \geq 0.05$) and be hadronic ($EMF < 0.95$). Its P_t must be greater than 25 GeV/c. The veto on isolated electrons and muons is performed. The $\not{E}_T$ isolation cuts **3J8** and **3J9** are the same as in the gluino analysis. $\not{E}_T$ is then required to be greater than 100 GeV. The final cut on H_T is optimized. The optimal value is obtained at 325 GeV. Five events are selected in the data. The distributions of $\not{E}_T$ after all cuts except **3J10**, and the distribution of H_T just before the cut **3J11**, are shown on Fig. 7. The number of events remaining at each step is given in Table IX. The various Standard Model background contributions are listed in Table X. The main background contribution is $W \to \tau\nu + $ jet jet for which there is a large statistical uncertainty. The evolution of the efficiency at the various stages of the analysis is given in Table IX for $M_{\tilde{q}} = M_{\tilde{g}} = 325$ GeV/c^2, together with the numbers of events seen in the data. The final efficiencies as a function of the average squark and
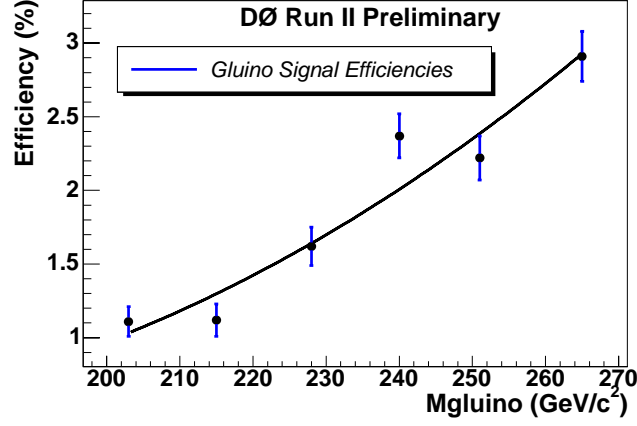
FIG. 6: Signal efficiencies in the "gluino" analysis as a function of the gluino mass. The efficiency is fitted with a 2nd order polynomial.

gluino mass are displayed in Table XI. To avoid statistical fluctuations, these efficiencies are fitted with a straight line as a function of the squark and gluino mass (Fig. 8). In the limit computation, the efficiency from the fit will be used rather than the single point efficiency.
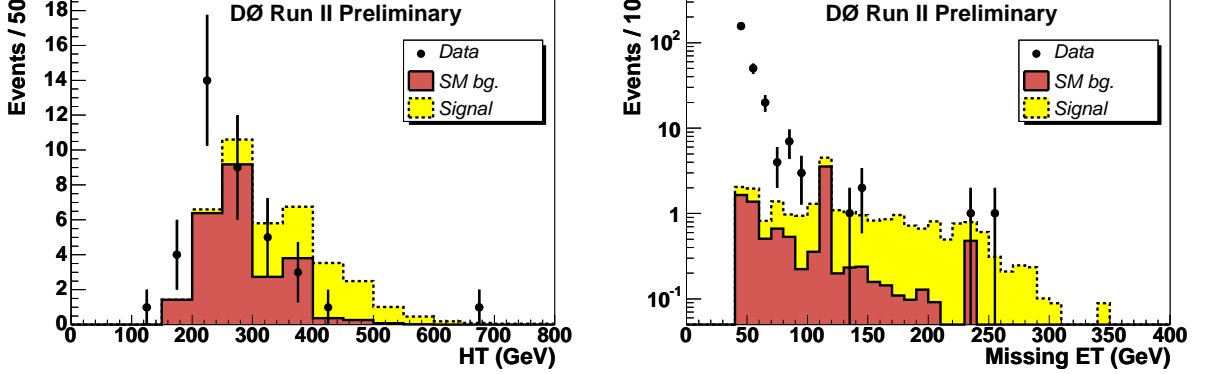

FIG. 7: "3 jets" analysis: Distribution of H_T just before the cuts **3J11** (left), and distribution of $\not{E}_T$ after all cuts except **3J10** (right) for data (points with error bars), for non-QCD standard model background (full histogram), and for signal Monte Carlo ($M_{\tilde{q}} = M_{\tilde{g}} = 325\,\mathrm{GeV}/c^2$; dashed histogram on top of SM).

TABLE IX: Number of data events and signal efficiencies for $M_{\tilde{q}} = M_{\tilde{g}} = 325\,\text{GeV}/c^2$ at the various stages of the "3 jets" analysis.

cut applied	events left	efficiency (%)
Common pre-selection	18,149	33.2
3J1 : at least 3 jets	16,267	29.6
3J2 : 3rd leading jet $|\eta_{\text{det}}| < 0.8$	7,221	16.7
3J3 : 3rd leading jet CPF > 0.05	7,113	16.6
3J4 : 3rd leading jet $P_t > 25$ GeV/c	4,460	13.8
3J5 : 3rd leading jet EMF < 0.95	4,399	13.0
3J6 : EM veto	4,323	12.3
3J7 : Muon veto	4,223	10.7
3J8 : $\Delta\Phi(MET, jet1) > 90$ degrees	3,952	10.1
3J9 : $\Delta\Phi(MET, jet2) > 50$ degrees	1,427	8.6
3J10: $\not{E}_T > 100$ GeV	38	6.7
3J11: $H_T > 325\,\text{GeV}$	5	5.1

TABLE X: Standard model processes and numbers of events expected in the "3 jets" analysis. The errors on the numbers of events expected are statistical only.

SM process	events expected
$Z \rightarrow \nu\bar{\nu} + 3\text{jets}$	0.4 ± 0.4
$W \rightarrow \tau\nu + \text{jet jet}$	3.0 ± 3.0
$Z \rightarrow \tau\tau + 2\text{jets}$	0.2 ± 0.2
$t\bar{t} \rightarrow b\bar{b}jjlnu$	2.3 ± 0.1
$t\bar{t} \rightarrow b\bar{b}lnulnu$	0.02 ± 0.01
$t\bar{t} \rightarrow b\bar{b}jjjj$	0.1 ± 0.1
QCD	negligible
total	6.1 ± 3.1

TABLE XI: Signal efficiencies and number of events expected in the "3 jets" analysis. The errors are statistical only.

$M_{\tilde{q}} = M_{\tilde{g}}$ (GeV/c^2)	efficiency (%)	events expected
290	3.46 ± 0.26	21.4 ± 1.6
295	3.84 ± 0.27	20.9 ± 1.5
300	4.31 ± 0.29	23.2 ± 1.5
305	4.50 ± 0.29	17.7 ± 1.2
310	5.19 ± 0.31	21.1 ± 1.3
315	4.61 ± 0.30	14.2 ± 0.9
320	5.05 ± 0.31	13.3 ± 0.8
325	5.10 ± 0.31	11.7 ± 0.7
330	5.80 ± 0.33	11.5 ± 0.7
335	5.72 ± 0.33	9.7 ± 0.6
340	6.43 ± 0.36	9.6 ± 0.5

V. RESULTS

A. Systematic uncertainties

The main experimental systematic errors are fully correlated between signal and SM backgrounds:

- a 6.5% uncertainty on the integrated luminosity;

- the uncertainties in the data and Monte Carlo jet energy scales. These were added in quadrature and yield:
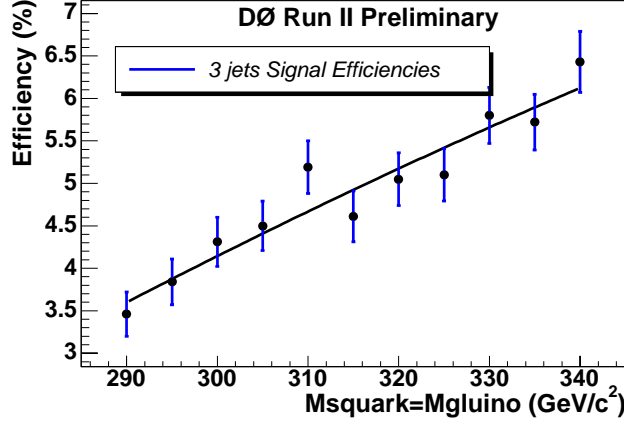
FIG. 8: Signal efficiencies in the "3 jets" analysis as a function of the squark and gluino masses. The efficiency is fitted with a straight line.

- "Dijet" analysis:
  a $^{+14}_{-11}$% relative uncertainty on the signal efficiency, and a $^{+24}_{-16}$% uncertainty on the SM background prediction.

- "Gluino" analysis:
  a $^{+0}_{-28}$% relative uncertainty on the signal efficiency, and a $^{+8}_{-20}$% uncertainty on the SM background prediction.

- "3 jets" analysis:
  a $^{+0}_{-31}$% relative uncertainty on the signal efficiency, and a $^{+11}_{-11}$% uncertainty on the SM background prediction.

- The systematic errors affecting the SM background cross sections were evaluated to be 7.5%.

Table XII summarizes the number of events observed and expected in the three analyses with both statistical and systematic uncertainties.

B.   Limits

Given

- the number of events selected

- the background expectations

- the signal efficiencies

- the above discussed systematic uncertainties, and

- the integrated luminosity of $310 \pm 20 \, \mathrm{pb}^{-1}$,

cross section upper limits at 95% confidence level (CL) have been obtained for the sets of mSUGRA parameters considered ($\tan\beta = 3$, $A_0 = 0$, $\mu < 0$), using the CL_s approach [11] with correlations between systematic errors properly taken into account. The observed cross section upper limit is shown in Fig. 9 as a function of the average squark mass or the gluino mass, together with theoretical expectations. Those were calculated at next-to-leading order [9], using the CTEQ5M PDF's, and for renormalization and factorization scales, μ, equal to $m_{\tilde{g}}$ (central value), $m_{\tilde{g}}/2$ and $2m_{\tilde{g}}$. In addition, the error on the NLO cross section of the central value ($\mu = m_{\tilde{g}}$) returned by the PROSPINO program was combined quadratically with the difference between the NLO cross section of the central value and the NLO cross section of the extreme cases ($\mu = m_{\tilde{g}}/2$ or $\mu = 2m_{\tilde{g}}$). For the central value (i.e. a renormalization scale equal to $m_{\tilde{g}}$):

- The "dijet" analysis excludes squark masses below $318\,\mathrm{GeV}/c^2$ for $m_0 = 25\,\mathrm{GeV}/c^2$.

- The "gluino" analysis excludes gluino masses below $233\,\mathrm{GeV}/c^2$ for $m_0 = 500\,\mathrm{GeV}/c^2$.

- The "3 jets" analysis excludes squark and gluino masses below $333\,\mathrm{GeV}/c^2$ for $M_{\tilde{q}} = M_{\tilde{g}}$.

These limits are $310\,\mathrm{GeV}/c^2$, $223\,\mathrm{GeV}/c^2$ and $322\,\mathrm{GeV}/c^2$ respectively for the worst case ($\mu = 2m_{\tilde{g}}$). The kinematic properties of the event with the largest missing E_T, selected by the "dijet" analysis, are given in Table XIII. Displays are presented in Figs. 10.

C. mSUGRA parameter scan

Signal points were generated in addition to the ones described in Table II to determine an excluded contour in the gluino/squark mass plane. These Monte Carlo events were generated under the same conditions as before (section III B): $\tan\beta = 3$, $A_0 = 0$, $\mu < 0$. Table XIV shows for each point the values of $(m_0, m_{1/2})$, which analysis has been used and the number of signal events expected with all errors. It also indicates if this point is excluded or not at the 95% confidence level. These results were obtained under the same conditions as described in Section V B. In particular, the central value of the renormalization and factorization scale ($\mu = m_{\tilde{g}}$) is used for the squark and gluino cross sections. Fig. 11 shows the excluded contour in the gluino/squark mass plane obtained from all results presented in this note. It improves previous limits on squark and gluino masses in the mSUGRA model.

TABLE XII: Numbers of events observed and expected in the 3 analyses. For the signals, the first column gives $(m_0, m_{1/2})$ in GeV/c^2 (for "dijet" and "gluino" analysis) or the squark and gluino mass in GeV/c^2 (for the "3 jets" analysis). The different errors correspond to the statistical error (stat.), the systematic error from cross section (x-sec), the systematic error from jet energy scale (JES), the systematic error from the luminosity measurement (lumi.), and from the QCD background determination (QCD). The last column indicates if this point is excluded or not at the 95% confidence level.

"dijet" analysis						
data	12					
back. sum	12.8	± 5.4 (stat.)	± 1.0 (x-sec)	$^{+3.1}_{-2.1}$ (JES)	± 0.8 (lumi.)	
(25,100)	58.4	± 5.5 (stat.)		$^{+8.2}_{-6.4}$ (JES)	± 3.8 (lumi.)	yes
(25,105)	55.8	± 4.6 (stat.)		$^{+7.8}_{-6.1}$ (JES)	± 3.6 (lumi.)	yes
(25,110)	49.0	± 3.6 (stat.)		$^{+6.9}_{-5.4}$ (JES)	± 3.2 (lumi.)	yes
(25,115)	43.1	± 2.9 (stat.)		$^{+6.0}_{-4.7}$ (JES)	± 2.8 (lumi.)	yes
(25,120)	37.1	± 2.4 (stat.)		$^{+5.2}_{-4.1}$ (JES)	± 2.4 (lumi.)	yes
(25,125)	31.3	± 1.9 (stat.)		$^{+4.4}_{-3.4}$ (JES)	± 2.0 (lumi.)	yes
(25,130)	25.4	± 1.5 (stat.)		$^{+3.6}_{-2.8}$ (JES)	± 1.7 (lumi.)	yes
(25,135)	21.9	± 1.3 (stat.)		$^{+3.1}_{-2.4}$ (JES)	± 1.4 (lumi.)	yes
(25,140)	17.8	± 1.0 (stat.)		$^{+2.5}_{-2.0}$ (JES)	± 1.2 (lumi.)	yes
(25,145)	14.3	± 0.8 (stat.)		$^{+2.0}_{-1.6}$ (JES)	± 0.9 (lumi.)	no
(25,150)	11.8	± 0.6 (stat.)		$^{+1.7}_{-1.3}$ (JES)	± 0.8 (lumi.)	no
(25,155)	9.9	± 0.5 (stat.)		$^{+1.4}_{-1.1}$ (JES)	± 0.6 (lumi.)	no
(25,160)	7.8	± 0.4 (stat.)		$^{+1.1}_{-0.9}$ (JES)	± 0.5 (lumi.)	no
"gluino" analysis						
data	10					
back. sum	7.1	± 0.9 (stat.)	± 0.4 (x-sec)	$^{+0.4}_{-1.1}$ (JES)	± 0.4 (lumi.) ± 0.4 (QCD)	
(500,65)	24.7	± 2.4 (stat.)		$^{+0.0}_{-6.9}$ (JES)	± 1.6 (lumi.)	yes
(500,70)	20.8	± 1.8 (stat.)		$^{+0.0}_{-5.8}$ (JES)	± 1.4 (lumi.)	yes
(500,75)	16.4	± 1.3 (stat.)		$^{+0.0}_{-4.6}$ (JES)	± 1.1 (lumi.)	yes
(500,80)	14.0	± 1.0 (stat.)		$^{+0.0}_{-3.9}$ (JES)	± 0.9 (lumi.)	no
(500,85)	11.6	± 0.8 (stat.)		$^{+0.0}_{-3.3}$ (JES)	± 0.8 (lumi.)	no
(500,90)	9.3	± 0.5 (stat.)		$^{+0.0}_{-2.6}$ (JES)	± 0.6 (lumi.)	no
"3 jets" analysis						
data	5					
back. sum	6.1	± 3.1 (stat.)	± 0.5 (x-sec)	$^{+0.7}_{-0.7}$ (JES)	± 0.4 (lumi.)	
290	22.5	± 1.6 (stat.)		$^{+0.0}_{-7.0}$ (JES)	± 1.5 (lumi.)	yes
295	21.1	± 1.5 (stat.)		$^{+0.0}_{-6.5}$ (JES)	± 1.4 (lumi.)	yes
300	19.0	± 1.3 (stat.)		$^{+0.0}_{-5.9}$ (JES)	± 1.2 (lumi.)	yes
305	17.3	± 1.1 (stat.)		$^{+0.0}_{-5.4}$ (JES)	± 1.1 (lumi.)	yes
310	16.4	± 1.1 (stat.)		$^{+0.0}_{-5.1}$ (JES)	± 1.1 (lumi.)	yes
315	15.0	± 0.9 (stat.)		$^{+0.0}_{-4.7}$ (JES)	± 1.0 (lumi.)	yes
320	13.6	± 0.8 (stat.)		$^{+0.0}_{-4.2}$ (JES)	± 0.9 (lumi.)	yes
325	12.4	± 0.7 (stat.)		$^{+0.0}_{-3.8}$ (JES)	± 0.8 (lumi.)	yes
330	11.2	± 0.7 (stat.)		$^{+0.0}_{-3.5}$ (JES)	± 0.7 (lumi.)	yes
335	10.1	± 0.6 (stat.)		$^{+0.0}_{-3.1}$ (JES)	± 0.7 (lumi.)	no
340	9.2	± 0.5 (stat.)		$^{+0.0}_{-2.8}$ (JES)	± 0.6 (lumi.)	no

TABLE XIII: Kinematic properties of the event with the largest missing E_T. Energies are in GeV, momenta in GeV/c, and angles in radians.

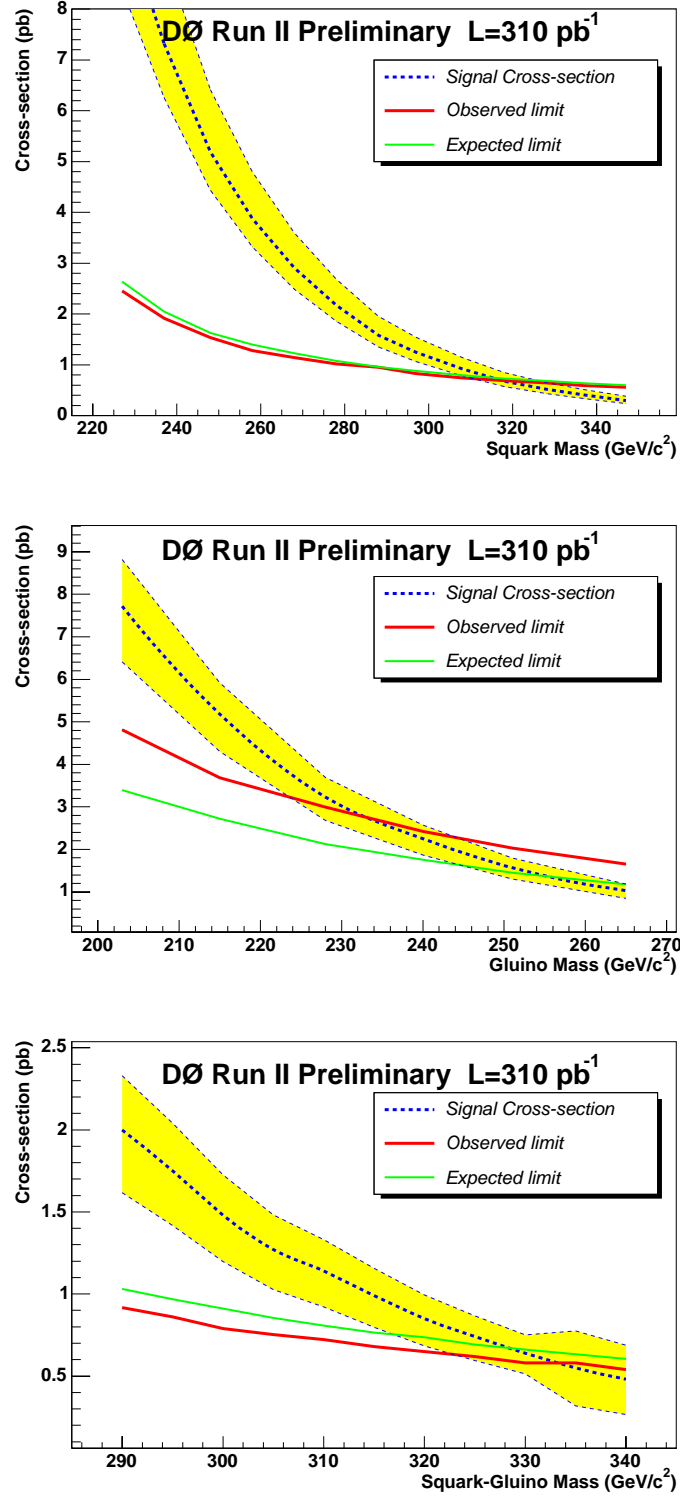|	p_T	η	ϕ
$\slashed{E}_T$	354		2.24
H_T	431		
Jet 1	264	-0.21	5.66
Jet 2	106	0.53	4.78
Jet 3	11.9	-1.55	4.26
Jet 4	11.0	-0.10	1.59

FIG. 9: Upper limits at the 95% confidence level on the squark and gluino production cross sections (red lines): as a function of the average squark mass from the "dijet" analysis (upper) for $m_0 = 25\,\mathrm{GeV}/c^2$; as a function of the gluino mass from the "gluino" analysis (middle) for $m_0 = 500\,\mathrm{GeV}/c^2$; as a function of the squark and gluino mass from the "3 jets" analysis (bottom) for $M_{\tilde{q}} = M_{\tilde{g}}$. The signal NLO cross sections are indicated by the dashed blue lines for $\tan\beta = 3$, $A_0 = 0$, $\mu < 0$. For the central line, the renormalization and factorization scale is $\mu = m_{\tilde{g}}$. For the two other lines, $\mu = m_{\tilde{g}}/2$ and $\mu = 2m_{\tilde{g}}$. The difference between the central line and the other two also includes the error on the K-factor computed by PROSPINO.

FIG. 10: Displays of the event with the largest missing E_T: xy view (top, left), lego plot (top, right), Rz view (bottom, left) and 3D-view (bottom, right).

TABLE XIV: Numbers of signal events expected for the additional points in the mSUGRA parameter scanning. The first column gives $(m_0, m_{1/2})$ in GeV/c^2. The second indicates which analysis has been used for this point. The different errors correspond to the statistical error (stat.), the systematic error from jet energy scale (JES) and the systematic error from the luminosity measurement (lumi.). The last column indicates if this point is excluded or not at the 95% confidence level.

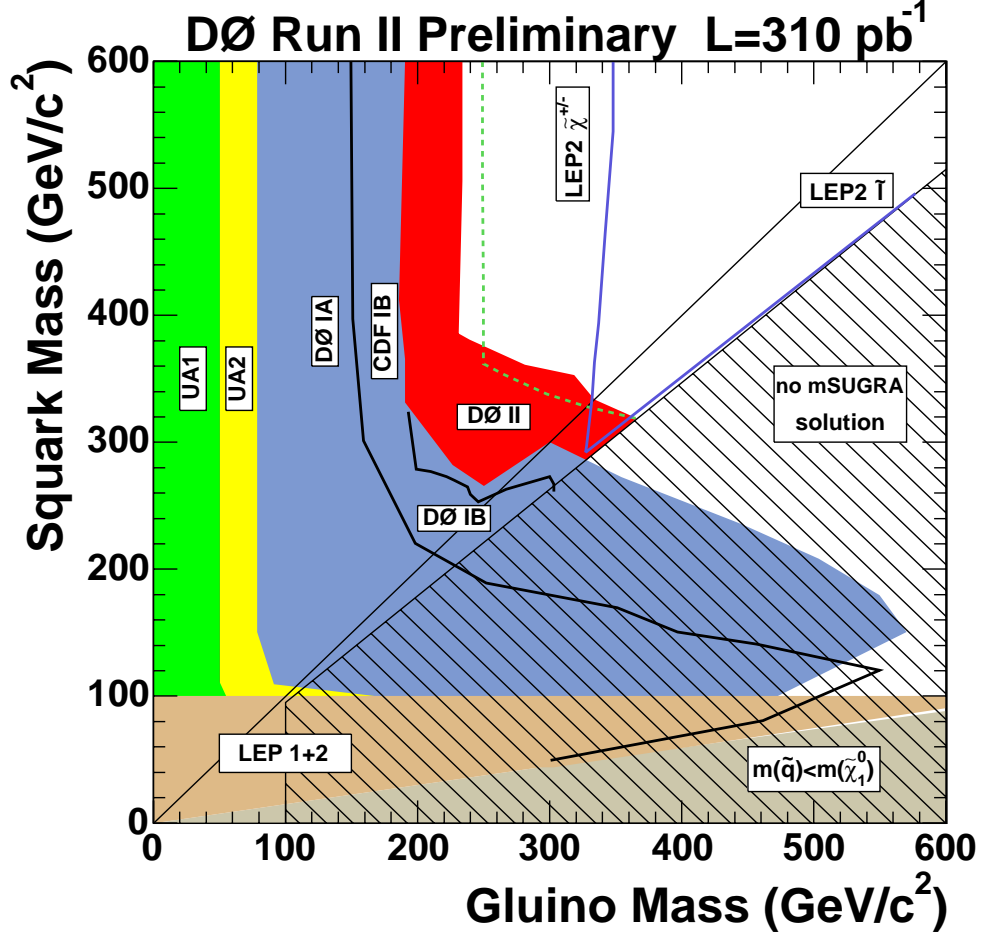|						
(200,100)	"3 jets"	27.0	±2.0 (stat.)	$^{+0.0}_{-7.6}$ (JES)	±1.8 (lumi.)	yes
(200,110)	"3 jets"	18.7	±1.3 (stat.)	$^{+0.0}_{-5.2}$ (JES)	±1.2 (lumi.)	yes
(200,120)	"3 jets"	14.2	±0.9 (stat.)	$^{+0.0}_{-4.0}$ (JES)	±0.9 (lumi.)	yes
(250,90)	"3 jets"	25.6	±2.0 (stat.)	$^{+0.0}_{-7.2}$ (JES)	±1.7 (lumi.)	yes
(250,100)	"3 jets"	16.9	±1.2 (stat.)	$^{+0.0}_{-4.7}$ (JES)	±1.1 (lumi.)	yes
(250,110)	"3 jets"	12.2	±0.8 (stat.)	$^{+0.0}_{-3.4}$ (JES)	±0.8 (lumi.)	yes
(250,120)	"3 jets"	10.0	±0.5 (stat.)	$^{+0.0}_{-2.8}$ (JES)	±0.6 (lumi.)	no
(300,75)	"3 jets"	25.2	±2.6 (stat.)	$^{+0.0}_{-7.1}$ (JES)	±1.6 (lumi.)	yes
(300,85)	"3 jets"	17.2	±1.5 (stat.)	$^{+0.0}_{-4.8}$ (JES)	±1.1 (lumi.)	yes
(300,95)	"3 jets"	12.1	±0.9 (stat.)	$^{+0.0}_{-3.4}$ (JES)	±0.8 (lumi.)	no
(350,75)	"3 jets"	12.6	±1.7 (stat.)	$^{+0.0}_{-3.5}$ (JES)	±0.8 (lumi.)	yes
(350,85)	"3 jets"	10.1	±1.0 (stat.)	$^{+0.0}_{-2.8}$ (JES)	±0.7 (lumi.)	yes
(350,95)	"3 jets"	8.6	±0.7 (stat.)	$^{+0.0}_{-2.4}$ (JES)	±0.6 (lumi.)	no
(400,75)	"gluino"	17.3	±1.9 (stat.)	$^{+0.0}_{-4.8}$ (JES)	±1.1 (lumi.)	yes
(400,85)	"gluino"	12.6	±1.1 (stat.)	$^{+0.0}_{-3.5}$ (JES)	±0.8 (lumi.)	no
(400,95)	"gluino"	7.4	±0.6 (stat.)	$^{+0.0}_{-2.1}$ (JES)	±0.5 (lumi.)	no

FIG. 11: In the squark and gluino mass plane, excluded regions at the 95% confidence level in the mSUGRA framework for $\tan\beta = 3$, $A_0 = 0$, $\mu < 0$. The green region was excluded by UA1 [12], the yellow one by UA2 [13], the brown one by the LEP experiments [15] and the blue one by CDF Run Ib [2]. The black contours correspond to the excluded regions obtained by DØ Run Ia [14] and DØ Run Ib [1]. In the grey region, the squark mass is lower than the mass of the lightest neutralino. There is no mSUGRA solution in the black hashed region. The two blue lines indicate the limits inferred from the LEP2 chargino and slepton searches [15]. The red region is excluded by the present analysis, using 310 pb^{-1} of DØ Run II data. The corresponding expected limit is the dashed green line.

Acknowledgments

[1] DØ Collaboration, B. Abbott *et al.*, *"Search for Squarks and Gluinos in Events Containing Jets and a Large Imbalance in Transverse Momentum"*, Phys. Rev. Lett. **83** (1999) 4937.

[2] CDF Collaboration, T. Affolfer *et al.*, *"Search for Gluinos and Scalar Quarks in $p\bar{p}$ Collisions at $\sqrt{s} = 1.8\,TeV$ using the Missing Energy plus Multijets Signature"*, Phys. Rev. Lett. **88** (2002) 041801.

[3] H.P. Nilles, Phys. Rep. **110** (1984) 1.

[4] M.L. Mangano *et al.*, *"ALPGEN, a generator for hard multiparton processes in hadronic collisions"*, JHEP **0307** (2003) 001.

[5] T. Sjöstrand *et al.*, Computer Phys. Commun. **135** (2001) 238.

[6] J. Pumplin *et al.*, JHEP **0207** (2002) 012,
D. Stump *et al.*, JHEP **0310** (2003) 046.

[7] J. Campbell and K. Ellis, *"MCFM - Monte Carlo for FeMtobarn processes"*, http://mcfm.fnal.gov/.

[8] N. Kidonakis and R. Vogt, Int. Mod. Phys. **A19** (2004) 1793.

[9] W. Beenakker, R. Hopker and M. Spira, *"PROSPINO: A program for the production of supersymmetric particles in next-to-leading order QCD"*, [hep-ph/9611232]

[10] H. Baer, F.E. Paige, S.D. Protopopescu and X. Tata, *"ISAJET: A Monte Carlo Event Generator for pp, $\bar{p}p$, and e^+e^- Interactions"*, hep-ph/0312045.

[11] The ALEPH, DELPHI, L3 and OPAL Collaborations and the LEP Working Group for Higgs boson searches, R. Barate *et al.*, *"Search for the Standard Model Higgs Boson at LEP"*, Phys. Lett. **B565** (2003) 61.

[12] UA1 Collaboration, C. Albajar *et al.*, *"Events With Large Missing Transverse Energy at the CERN Collider (Paper 3): Mass Limits On Supersymmetric Particles"*, Phys. Lett. **B198** (1987) 261.

[13] UA2 Collaboration, J. Alitti *et al.*, *" A Search for Squark And Gluino Production at the CERN Anti-P P Collider"*, Phys. Lett. **B235** (1990) 363.

[14] DØ Collaboration, S. Abachi *et al.*, *Search for squarks and gluinos in p anti-p collisions at sqrts = 1.8 TeV*, Phys. Rev. Lett. **75** (1995) 618.

[15] LEP SUSY Working Group for the ALEPH, DELPHI, L3 and OPAL collaborations,
http://lepsusy.web.cern.ch/lepsusy/